nature

Accelerated Article Preview

Pathogenesis and transmission of SARS-CoV-2 in golden hamsters

Sin Fun Sia, Li-Meng Yan, Alex W. H. Chin, Kevin Fung, Ka-Tim Choy, Alvina Y. L. Wong, Prathanporn Kaewpreedee, Ranawaka A. P. M. Perera, Leo L. M. Poon, John M. Nicholls, Malik Peiris & Hui-Ling Yen

Article

Pathogenesis and transmission of SARS-CoV-2 in golden hamsters

Sin Fun Sia[1,3], Li-Meng Yan[1,3], Alex W. H. Chin[1,3], Kevin Fung[2], Ka-Tim Choy[1], Alvina Y. L. Wong[1], Prathanporn Kaewpreedee[1], Ranawaka A. P. M. Perera[1], Leo L. M. Poon[1], John M. Nicholls[2], Malik Peiris[1] & Hui-Ling Yen[1✉]

SARS-CoV-2, a novel coronavirus with high nucleotide identity to SARS-CoV and SARS-related coronaviruses detected in horseshoe bats, has spread across the world and impacted global healthcare systems and economy[1,2]. A suitable small animal model is needed to support vaccine and therapy development. We report the pathogenesis and transmissibility of the SARS-CoV-2 in golden Syrian hamsters. Immunohistochemistry demonstrated viral antigens in nasal mucosa, bronchial epithelial cells, and in areas of lung consolidation on days 2 and 5 post-inoculation (dpi), followed by rapid viral clearance and pneumocyte hyperplasia on 7 dpi. Viral antigen was also found in the duodenum epithelial cells with viral RNA detected in feces. Notably, SARS-CoV-2 transmitted efficiently from inoculated hamsters to naïve hamsters by direct contact and via aerosols. Transmission via fomites in soiled cages was less efficient. Although viral RNA was continuously detected in the nasal washes of inoculated hamsters for 14 days, the communicable period was short and correlated with the detection of infectious virus but not viral RNA. Inoculated and naturally-infected hamsters showed apparent weight loss, and all animals recovered with the detection of neutralizing antibodies. Our results suggest that SARS-CoV-2 infection in golden Syrian hamsters resemble features found in humans with mild infections.

SARS-CoV-2 was first detected from a cluster of pneumonia patients in Wuhan, Hubei Province, China in December 2019. Although 55% of the initial cases were linked to one seafood wholesale market where wild animals were also sold[3], multiple viral (sustained human-to-human transmissibility by symptomatic and pre-symptomatic patients[4]) and ecological factors (extensive domestic and international travel during Chinese Lunar New Year) have contributed to the rapid global spread of the virus. The clinical spectrum of patients with the novel coronavirus disease (COVID-19) is wide, 19% of 72,314 symptomatic patients in China progressed to severe and critical illness[5] with an estimated 1.4% symptomatic case fatality risk[6]. There is no approved vaccine or treatment against SARS-CoV-2, and the available interventions including country lock-down and social distancing have severely disrupted the global supply chain and economy.

A suitable animal model is essential for understanding the pathogenesis of this disease and for evaluating vaccine and therapeutic candidates. Previous animal studies on SARS-CoV suggested the importance of the interaction between the viral spike protein and the host angiotensin converting enzyme 2 (ACE2) receptors[7–10] as well as age and innate immune status of the animals[11–14] in pathogenesis. As with SARS-CoV, the spike protein of SARS-CoV-2 also utilizes ACE2 receptors that are distributed predominantly in the epithelial cells of the lungs and small intestine to gain entry into epithelial cells for viral replication[1,15]. SARS-CoV-2 showed good binding for human ACE2 but limited binding to murine

ACE2[1], which has limited the use of inbred mice for research. Macaques and transgenic ICR mice expressing human ACE2 receptor were shown to be susceptible for SARS-CoV-2 infection[16–18]; however, there is limited availability of these animal models. Cynomolgus macaques and rhesus macaques challenged with SARS-CoV-2 showed pneumonia with limited[17] and moderate[18] clinical signs, respectively. The challenged transgenic mice showed pneumonia moderate weight loss, and no apparent histological changes in non-respiratory tissues[16]. Previously generated transgenic mice expressing human ACE2 receptor have been reported to support SARS-CoV replication in the airway epithelial cells but were associated with neurological-related mortality due to high ACE2 expression in the brain[7–10].

Golden Syrian hamster is a widely used experimental animal model and was reported to support replication of SARS-CoV[19,20] but not MERS-CoV[21], which utilizes the dipeptidyl peptidase-4 (DPP4) protein as the main receptor for viral entry. Previous study of SARS-CoV (Urbani strain) in 5-weeks-old golden Syrian hamsters showed robust viral replication with peak viral titers detected in the lungs on 2 dpi, followed by rapid viral clearance by 7 dpi, but without weight loss or evidence of disease in the inoculated animals[20]. A follow up study reported testing different strains of SARS-CoV in golden Syrian hamsters and found differences in virulence between SARS-CoV strains; lethality was reported in hamsters challenged with the Frk-1 strain, which differed from the non-lethal Urbani strain by the L1148F mutation in the S2

[1]School of Public Health, Li Ka Shing Faculty of Medicine, The University of Hong Kong, Hong Kong, China. [2]Department of Pathology, Li Ka Shing Faculty of Medicine, The University of Hong Kong, Hong Kong, China. [3]These authors contributed equally: Sin Fun Sia, Li-Meng Yan, Alex W. H. Chin. ✉e-mail: hyen@hku.hk

Article

domain[19]. Hamsters are permissive for infection by other respiratory viruses including human metapneumovirus[22], human parainfluenza virus 3[23] and influenza A virus and may support influenza transmission by contact or airborne routes[24,25]. Alignment of the ACE2 protein of human, macaque, mice, and hamster suggest that the spike protein of SARS-CoV-2 may interact more efficiently with hamster ACE2 than murine ACE2 (Extended Data Fig. 1). Here, we evaluated the pathogenesis and contact transmissibility of SARS-CoV-2 in 4-5 weeks old male golden Syrian hamsters.

Hamsters were infected intranasally with 8×10^4 $TCID_{50}$ of the Beta-CoV/Hong Kong/VM20001061/2020 virus (GISAID# EPI_ISL_412028) isolated in Vero E6 cells from the nasopharynx aspirate and throat swab of a confirmed COVID-19 patient in Hong Kong. On 2, 5, 7 dpi, nasal turbinate, brain, lungs, heart, duodenum, liver, spleen and kidney were collected to monitor viral replication and histopathological changes. Peak viral load in the lungs was detected on 2 dpi and decreased on 5 dpi; no infectious virus was detected on 7 dpi despite of the continued detection of high copies of viral RNA (Fig. 1a). Infectious viral load was significantly different between 2 and 7 dpi ($P= 0.019$, Dunn's multiple comparisons test) but not the RNA copy number ($P= 0.076$). No infectious virus was detected in the kidney although low copies of viral RNA were detected on 2 and 5 dpi (Fig. 1b).

Histopathological examination detected an increase in inflammatory cells and consolidation in 5-10% of the lungs on 2 dpi (Fig. 1c, 1d) and 15-35% of the lungs on 5 dpi (Fig. 1e, 1f). Mononuclear cell infiltrate was observed in areas where viral antigen was detected on 2 and 5 dpi. Immunohistochemistry for SARS-CoV-2 N protein demonstrated viral antigen in the bronchial epithelial cells on 2 dpi (Fig. 1d) with progression to pneumocytes on 5 dpi (Fig. 1f). On 7 dpi, there was an increased consolidation in 30-60% of the lungs (Fig. 1g); however, no viral antigen was detected (Fig. 1h) and type 2 pneumocyte hyperplasia was prominent (Extended Data Fig. 2a). CD3 positive T lymphocytes were detected in the peri-bronchial region on 5 dpi, which may facilitate the rapid clearance of the infected cells (Extended Data Fig. 2b). There was moderate inflammatory cell infiltration in the nasal turbinate (Fig. 1i), and viral antigen was detected in the nasal epithelial cells (Fig. 1j) and in olfactory sensory neurons at the nasal mucosa (Fig. 1j). Infection in the olfactory neurons was further confirmed in cells expressing both SARS-CoV-N protein and neuron-specific beta-III tubulin (Extended Data Fig. 2c). Compared to mock infection (Extended Data Fig. 2d and 2e), infection lead to a reduction in the number of olfactory neurons at the nasal mucosal on 2 dpi (Extended Data Fig. 2f), prominent nasal epithelial attenuation on 7 dpi (Extended Data Figure 2g), followed by tissue repairing on 14 dpi (Extended data Figure 2h). Though no inflammation was present (Fig. 1k), viral antigen was detected from the epithelial cells of duodenum on 2 dpi (Fig. 1l). This resembles the detection of SARS-CoV virus replication in the epithelial cells of terminal ileum and colon of SARS-CoV patients without observing apparent architectural disruption and inflammatory infiltrate[26]. No apparent histopathological change was observed from brain, heart, liver, and kidney on 5 dpi (Extended Data Fig. 2i, 2j, 2k, 2l).

To assess the transmission potential of the SARS-CoV-2 in hamsters, three donor hamsters were inoculated intra-nasally with 8×10^4 $TCID_{50}$ of the virus. At 24h post-inoculation, each donor was transferred to a new cage and co-housed with one naïve hamster. Weight changes and clinical signs were monitored daily and nasal washes were collected every other day from donors and contacts for 14 days. In donors, the peak infectious viral load in nasal washes was detected early post-inoculation followed by a rapid decline, although viral RNA was continuously detected for 14 days (Fig. 2a). Hamsters inoculated with the SARS-CoV-2 showed the maximal mean weight loss (mean ± SD, -11.97 ± 4.51%, N=6) on 6 dpi (Fig. 2b). Transmission from donors to co-housed contacts was efficient, and SARS-CoV-2 was detected from the co-housed hamsters on day 1 post-contact (dpc), with the peak viral load in nasal washes detected on 3 dpc (Fig. 2c). The total

viral load shed in the nasal washes was approximated by calculating the area under the curve (AUC) for each animal. The contact hamsters shed comparable amount of virus in the nasal washes compared to the donor hamsters ($P= 0.1$, two-tailed Mann-Whitney test). Contact hamsters showed the maximal mean weight loss (mean ± SD, -10.68 ± 3.42%, N=3) on 6 dpc; all animals returned to the original weight after 11 dpc (Fig. 2d). Neutralizing antibody were detected using plaque reduction neutralization (PRNT) assay from donors on 14 dpi (titers at 1:640 for all) and from contacts on 13 dpc (titers at 1:160, 1:320, and 1:160). As viral RNA was continuously detected from the donor's nasal washes for 14 days while infectious virus titers decreased rapidly, we repeated the experiment and co-housed naïve contacts with donors on 6 dpi. Low quantity of viral RNA was detected in the nasal washes in one contact on 3 and 7 dpc without detection of infectious virus in the nasal washes (Fig. 2e), and none of the contact hamsters showed weight loss (Fig. 2f). PRNT assay detected no neutralizing antibody (< 1:10) from the contact animals on 12 dpc. The results suggest that the SARS-CoV-2 inoculated donors have a short communicable period of less than 6 days. Onward transmissibility from donors to co-housed contacts was correlated with the detection of infectious virus but not viral RNA in the donor nasal washes.

Transmission from donor to co-housed contact may be mediated by multiple transmission routes. To investigate the transmissibility of SARS-CoV-2 among hamsters via aerosols, donors and naïve aerosol contacts were placed in two adjacent wire cages for 8 hours on 1 dpi (Extended Data Fig. 3). The experiment was performed in three pairs of donor: aerosol contact at 1:1 ratio. The animals were single-housed after exposure and were monitored daily for 14 days. Donor hamsters shed infectious virus in the nasal washes for 6 days, while viral RNA can be continuously detected for 14 days (Fig. 3a). Viral RNA was detected in the donors' fecal samples on 2, 4, 6 dpi without detection of infectious virus (Fig. 3b). Donors showed comparable weight loss (Fig. 3c) as observed previously (Fig. 2b). Transmission via aerosols was efficient as infectious virus was detected in the nasal washes from all exposed contacts on 1 dpc, with peak viral loads detected on 3 dpc (Fig. 3d). Viral RNA was continuously detected from the fecal samples of the infected aerosol contacts for 14 days, although no infectious virus was isolated (Fig. 3e). The aerosol contact animals showed the maximal weight loss (mean ± SD, -7.72 ± 5,42%, N=3) on 7 dpc (Fig. 3f). The aerosol contact hamsters shed comparable amount of virus in the nasal washes (approximated by AUC) compared to the donor hamsters ($P= 0.4$, two-tailed Mann-Whitney test). PRNT assay detected neutralizing antibody from the donors on 16 dpi (titers at 1:320, 1:640, 1:640) and the contacts on 15 dpc (titers at 1:640 for all). To evaluate transmission potential of SARS-CoV-2 via fomites, three naïve fomite contacts were each introduced to a soiled cage housed by one donor from 0 to 2 dpi. The fomite contact hamsters were single-housed in the soiled cages for 48 hours and were each transferred to a new cage on 2 dpc (equivalent to 4 dpi of the donors). Viral RNA was detected from different surfaces sampled from the soiled cages used for housing the fomite contacts, with low titer of infectious virus detected from the bedding (2 dpi), cage side surface (4dpi), and water bottle nozzle (4 dpi) (Extended Data table 1). One out of three fomite contacts shed infectious virus in the nasal washes starting from 1 dpc with the peak viral load detected on 3 dpc (Fig. 3g). Viral RNA but not infectious virus was detected from the fecal samples (Fig. 3h). The maximal weight loss was 8.79% on 7 dpc (Fig. 3i). PRNT assay detected neutralizing antibody from the sera of one out of three fomite contacts on 16 dpc (titers at 1:320). Taken together, these results suggest that transmission of SARS-CoV-2 among hamsters were mainly mediated via aerosols than via fomites.

Our results indicate that the golden Syrian hamster is a suitable experimental animal model for SARS-CoV-2, as there is apparent weight loss in the inoculated and naturally-infected hamsters and evidence of efficient viral replication in the nasal mucosa and lower respiratory epithelial cells. The ability of SARS-CoV-2 to infect olfactory sensory

neurons at the nasal mucosa may explain the anosmia reported in COVID-19 patients. Hamsters support efficient transmission of SARS-CoV-2 from inoculated donors to naïve hamsters by direct contact or via aerosols. We also show that transmission from the donors to naïve hamsters may occur within a short period early post-inoculation. Our findings are consistent with a recent report[27] while the current study was under peer review. Hamsters are easy to handle and there are reagents to support immunological studies for vaccine development[28–30]. The results also highlighted similarity and differences between the SARS-CoV and SARS-CoV-2 in the hamster model. Both viruses replicated efficiently in the respiratory epithelial cells with peak viral load detected early post-inoculation, followed by infiltration of mononuclear inflammatory cells in the lungs and rapid clearance of infectious virus by 7 dpi. Understanding the host defense mechanism leading to the rapid viral clearance in the respiratory tissues of the hamsters may aid the development of effective counter measures for SARS-CoV-2. The efficient transmission of SARS-CoV-2 to naïve hamsters by aerosols also provide opportunities to understand the transmission dynamics for this novel coronavirus.

Online content

Any methods, additional references, Nature Research reporting summaries, source data, extended data, supplementary information, acknowledgements, peer review information; details of author contributions and competing interests; and statements of data and code availability are available at https://doi.org/10.1038/s41586-020-2342-5.

1. Zhou, P. et al. A pneumonia outbreak associated with a new coronavirus of probable bat origin. Nature, https://doi.org/10.1038/s41586-020-2012-7 (2020).
2. WHO. Coronavirus disease (COVID-2019) situation reports, https://www.who.int/emergencies/diseases/novel-coronavirus-2019/situation-reports (2020).
3. Li, Q. et al. Early Transmission Dynamics in Wuhan, China, of Novel Coronavirus-Infected Pneumonia. N Engl J Med, https://doi.org/10.1056/NEJMoa2001316 (2020).
4. He, X. et al. Temporal dynamics in viral shedding and transmissibility of COVID-19. Nat Med, https://doi.org/10.1038/s41591-020-0869-5 (2020).
5. Wu, Z. & McGoogan, J. M. Characteristics of and Important Lessons From the Coronavirus Disease 2019 (COVID-19) Outbreak in China: Summary of a Report of 72314 Cases From the Chinese Center for Disease Control and Prevention. JAMA, https://doi.org/10.1001/jama.2020.2648 (2020).
6. Wu, J. T. et al. Estimating clinical severity of COVID-19 from the transmission dynamics in Wuhan, China. Nature Medicine, https://doi.org/10.1038/s41591-020-0822-7 (2020).
7. McCray, P. B., Jr. et al. Lethal infection of K18-hACE2 mice infected with severe acute respiratory syndrome coronavirus. J Virol 81, 813-821, https://doi.org/10.1128/JVI.02012-06 (2007).
8. Menachery, V. D. et al. SARS-like WIV1-CoV poised for human emergence. Proc Natl Acad Sci U S A 113, 3048-3053, https://doi.org/10.1073/pnas.1517719113 (2016).
9. Tseng, C. T. et al. Severe acute respiratory syndrome coronavirus infection of mice transgenic for the human Angiotensin-converting enzyme 2 virus receptor. J Virol 81, 1162-1173, https://doi.org/10.1128/JVI.01702-06 (2007).
10. Yang, X. H. et al. Mice transgenic for human angiotensin-converting enzyme 2 provide a model for SARS coronavirus infection. Comp Med 57, 450-459 (2007).
11. Baas, T. et al. Genomic analysis reveals age-dependent innate immune responses to severe acute respiratory syndrome coronavirus. J Virol 82, 9465-9476, https://doi.org/10.1128/JVI.00489-08 (2008).
12. Glass, W. G., Subbarao, K., Murphy, B. & Murphy, P. M. Mechanisms of host defense following severe acute respiratory syndrome-coronavirus (SARS-CoV) pulmonary infection of mice. J Immunol 173, 4030-4039, https://doi.org/10.4049/jimmunol.173.6.4030 (2004).
13. Hogan, R. J. et al. Resolution of primary severe acute respiratory syndrome-associated coronavirus infection requires Stat1. J Virol 78, 11416-11421, https://doi.org/10.1128/JVI.78.20.11416-11421.2004 (2004).
14. Roberts, A. et al. Aged BALB/c mice as a model for increased severity of severe acute respiratory syndrome in elderly humans. J Virol 79, 5833-5838, https://doi.org/10.1128/JVI.79.9.5833-5838.2005 (2005).
15. Hamming, I. et al. Tissue distribution of ACE2 protein, the functional receptor for SARS coronavirus. A first step in understanding SARS pathogenesis. J Pathol 203, 631-637, https://doi.org/10.1002/path.1570 (2004).
16. Bao, L. et al. The Pathogenicity of SARS-CoV-2 in hACE2 Transgenic Mice, https://www.biorxiv.org/content/10.1101/2020.02.07.939389v3.full (2020).
17. Rockx, B. et al. Comparative pathogenesis of COVID-19, MERS, and SARS in a nonhuman primate model. Science, https://doi.org/10.1126/science.abb7314 (2020).
18. Munster, V. J. et al. Respiratory disease and virus shedding in rhesus macaques inoculated with SARS-CoV-2. bioRxiv, 2020.2003.2021.001628, https://doi.org/10.1101/2020.03.21.001628 (2020).
19. Roberts, A. et al. Animal models and vaccines for SARS-CoV infection. Virus Res 133, 20-32, https://doi.org/10.1016/j.virusres.2007.03.025 (2008).
20. Roberts, A. et al. Severe acute respiratory syndrome coronavirus infection of golden Syrian hamsters. J Virol 79, 503-511, https://doi.org/10.1128/JVI.79.1.503-511.2005 (2005).
21. de Wit, E. et al. The Middle East respiratory syndrome coronavirus (MERS-CoV) does not replicate in Syrian hamsters. PLoS One 8, e69127, https://doi.org/10.1371/journal.pone.0069127 (2013).
22. MacPhail, M. et al. Identification of small-animal and primate models for evaluation of vaccine candidates for human metapneumovirus (hMPV) and implications for hMPV vaccine design. J Gen Virol 85, 1655-1663, https://doi.org/10.1099/vir.0.79805-0 (2004).
23. Buthala, D. A. & Soret, M. G. Parainfluenza Type 3 Virus Infection in Hamsters: Virologic, Serologic, and Pathologic Studies. J Infect Dis 114, 226-234, https://doi.org/10.1093/infdis/114.3.226 (1964).
24. Ali, M. J., Teh, C. Z., Jennings, R. & Potter, C. W. Transmissibility of influenza viruses in hamsters. Arch Virol 72, 187-197, https://doi.org/10.1007/bf01348964 (1982).
25. Iwatsuki-Horimoto, K. et al. Syrian Hamster as an Animal Model for the Study of Human Influenza Virus Infection. J Virol 92, https://doi.org/10.1128/JVI.01693-17 (2018).
26. Leung, W. K. et al. Enteric involvement of severe acute respiratory syndrome-associated coronavirus infection. Gastroenterology 125, 1011-1017, https://doi.org/10.1016/s0016-5085(03)01215-0 (2003).
27. Chan, J. F. et al. Simulation of the clinical and pathological manifestations of Coronavirus Disease 2019 (COVID-19) in golden Syrian hamster model: implications for disease pathogenesis and transmissibility. Clin Infect Dis, https://doi.org/10.1093/cid/ciaa325 (2020).
28. Miao, J., Chard, L. S., Wang, Z. & Wang, Y. Syrian Hamster as an Animal Model for the Study on Infectious Diseases. Front Immunol 10, 2329, https://doi.org/10.3389/fimmu.2019.02329 (2019).
29. Warner, B. M., Safronetz, D. & Kobinger, G. P. Syrian Hamsters as a Small Animal Model for Emerging Infectious Diseases: Advances in Immunologic Methods. Adv Exp Med Biol 972, 87-101, https://doi.org/10.1007/5584_2016_135 (2017).
30. Zivcec, M., Safronetz, D., Haddock, E., Feldmann, H. & Ebihara, H. Validation of assays to monitor immune responses in the Syrian golden hamster (Mesocricetus auratus). J Immunol Methods 368, 24-35, https://doi.org/10.1016/j.jim.2011.02.004 (2011).
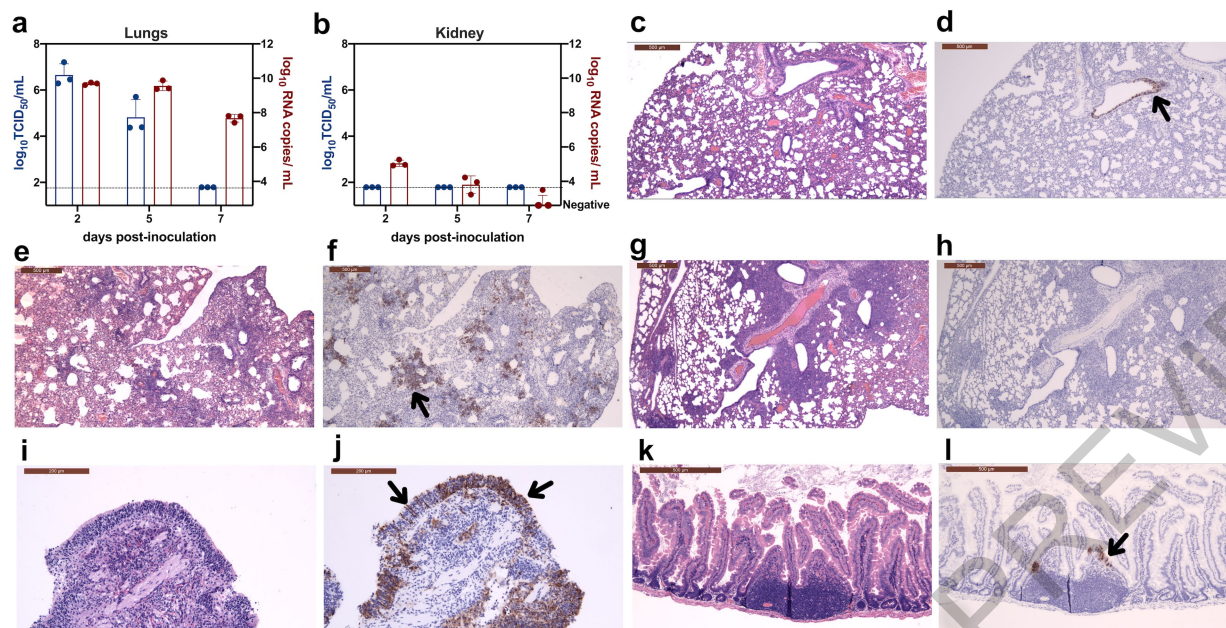
Fig. 1 | Viral load and histopathological changes in golden Syrian hamsters intranasally challenged with SARS-CoV-2. a, Infectious viral load (log_{10}TCID$_{50}$/mL) and viral RNA (log_{10} RNA copies/mL) detected in the lungs of SARS-CoV-2 challenged hamsters (N=3) on 2, 5, 7 dpi. **b**, Infectious viral load and viral RNA detected in the kidney of SARS-CoV-2 challenged hamsters (N=3) on 2, 5, 7 dpi. Individual data points and mean±SD were shown; the detection limit (1.789 log_{10} TCID$_{50}$/ mL) was shown with the dotted line. **c**, Haemotoxylin and eosin (H&E) staining of the lungs of SARS-CoV-2 challenged hamsters on 2 dpi. **d**, Detection of SARS-CoV-2 N protein at bronchial epithelial cells (indicated by an arrow) by immunohistochemistry on 2 dpi. **e**, H&E staining of the lungs on 5 dpi. **f**, Detection of N protein in pneumocytes with lung consolidation (indicated by an arrow) on 5 dpi. **g**, H&E staining of the lungs on 7 dpi. **h**, The lack of detection of N protein in the lungs on 7 dpi. **i**, H&E staining of nasal turbinate of challenged hamsters on 2 dpi. **j**, Detection of N protein in nasal epithelial cells (arrow on the right) and cells morphologically resembling olfactory neurons (arrow on the left) on 2 dpi. **k**, H&E staining of duodenum of challenged hamsters on 2 dpi. **l**, Detection of N protein in the duodenum epithelial cells on 2 dpi. The experiment was performed once with 9 hamsters challenged with 8 x 10⁴ TCID$_{50}$ of SARS-CoV-2, and tissues were collected from 3 animals for histopathology examination and immunohistochemistry at each time point. H&E staining and immunohistochemistry performed using tissues from three animals showed comparable results, and the representative images were shown.
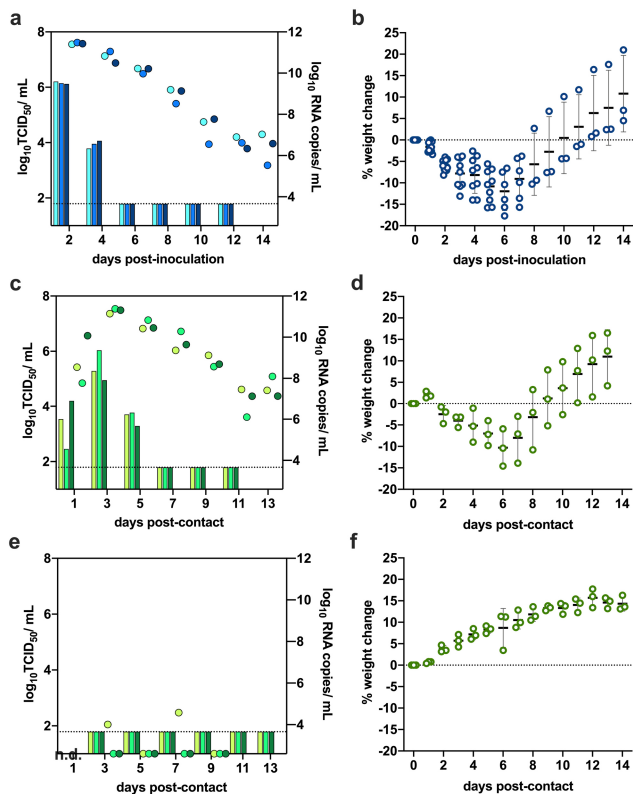
Fig. 2 | Transmission of SARS-CoV-2 in golden Syrian hamsters by direct contact. a, Infectious viral load ($\log_{10}$ TCID$_{50}$/mL, shown in bars) and viral RNA copy numbers ($\log_{10}$ RNA copies/mL, shown in color-matched dots) detected in the nasal washes of donor hamsters (N=3) inoculated with 8 x 10^4 TCID$_{50}$ of SARS-CoV-2. **b**, Body weight changes (% weight change compared to day 0) of hamsters inoculated with SARS-CoV-2 (N=9, including 3 donors and 9 challenged animals described in Fig. 1); individual data points and mean±SD were shown. **c**, Transmission of SARS-CoV-2 to naïve hamsters (N=3) that were each co-housed with one inoculated donor on 1 dpi; infectious viral load and viral RNA copy numbers detected in the nasal washes of contact hamsters were shown. **d**, Body weight changes (% weight change compared to the day of exposure) of contact hamsters (N=3) infected with SARS-CoV-2. **e**, Transmission of SARS-CoV-2 to naïve hamsters (N=3) that were each co-housed with one donor on 6 dpi; infectious viral load and viral RNA copy numbers detected in the nasal washes of contact hamsters were shown. **f**, Body weight changes of contact hamsters (N=3). Direct contact transmission experiments with co-housed donors with naïve contacts on 1 dpi and 6 dpi, respectively, were each performed once with three repeats.
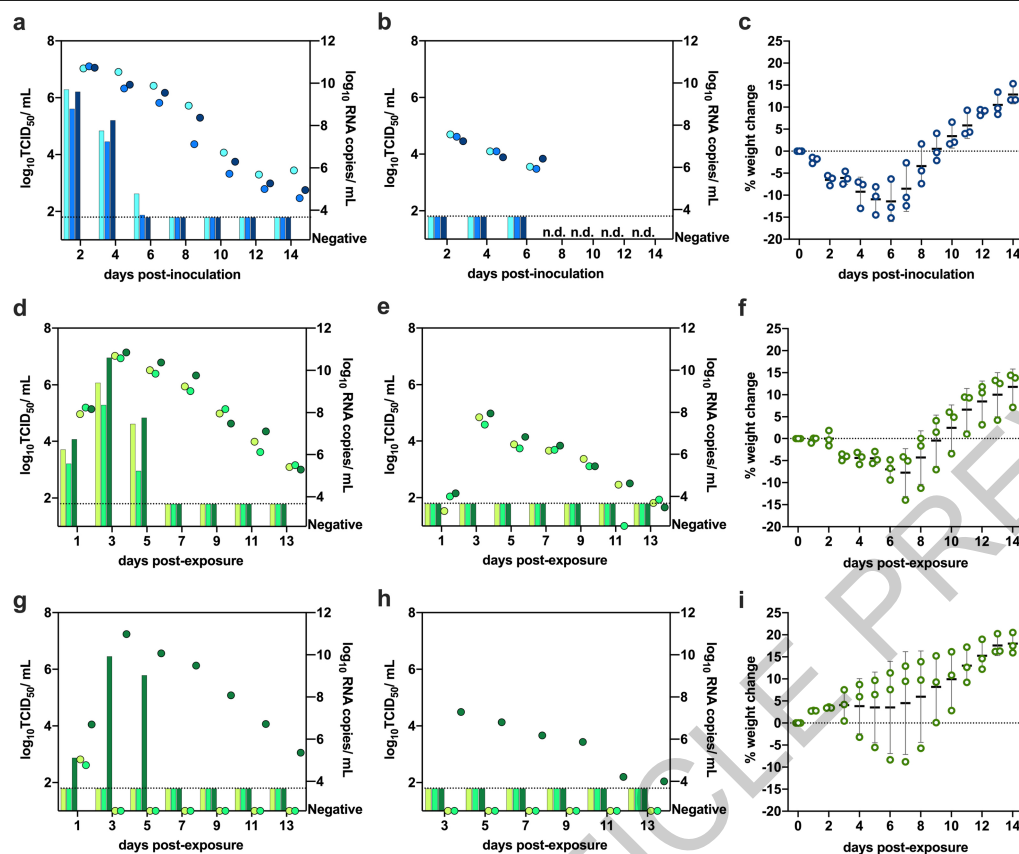
Fig. 3 | Transmission of SARS-CoV-2 in golden Syrian hamsters via aerosols and fomites. a, Infectious viral load ($\log_{10}TCID_{50}$/mL, shown in bars) and viral RNA copy numbers ($\log_{10}$ RNA copies/mL, shown in color-matched dots) detected in the nasal washes of donor hamsters (N=3) inoculated with 8×10^4 $TCID_{50}$ of SARS-CoV-2. **b**, Infectious virus and viral RNA detected in the fecal samples of donor hamsters (N=3). **c**, Body weight changes of donor hamsters (N=3); individual data points and mean±SD were shown. **d**, Aerosol transmission of SARS-CoV-2 to naïve hamsters (N=3) exposed to donors for 8 hours on 1 dpi; Infectious virus and viral RNA detected in the nasal washes of aerosol contact hamsters were shown. **e**, Infectious virus and viral RNA

detected in the fecal samples of aerosol contact hamsters (N=3). **f**, Body weight changes (% weight change compared to the day of exposure) of aerosol contact hamsters (N=3). **g**, Fomite transmission of SARS-CoV-2 to naïve hamsters (N=3) that were single-housed in donors' soiled cages for 48 hours; Infectious virus and viral RNA detected in the nasal washes of fomite contact hamsters were shown. **h**, Infectious virus and viral RNA detected in the fecal samples of fomite contact hamsters (N=3). **i**, Body weight changes (% weight change compared to the day of exposure) of fomite contact hamsters (N=3). Aerosol transmission and fomite transmission experiments were each performed once with three repeats.

Methods

Virus

BetaCoV/Hong Kong/VM20001061/2020 virus was isolated from a confirmed COVID-19 patient in Hong Kong in Vero E6 cells at the BSL-3 core facility, LKS Faculty of Medicine, The University of Hong Kong. Vero E6 cells were purchased from ATCC (CRL-1586) without further authentication, and the cells were routinely tested negative for *Mycoplasma sp.* by real-time PCR. Stock virus ($10^{7.25}$ TCID$_{50}$/mL) was prepared after three serial passages in Vero E6 cells in Dulbecco's Modified Eagle Medium (DMEM) supplemented with 4.5 g/L D-glucose, 100 mg/L sodium pyruvate, 2% FBS, 100,000 U/L Penicillin-Streptomycin, and 25mM HEPES.

Animal experiments

Male golden Syrian hamsters at 4-5 weeks old were obtained from Laboratory Animal Services Centre, Chinese University of Hong Kong. The hamsters were originally imported from Harlan (Envigo), UK in 1998. All experiments were performed at the BSL-3 core facility, LKS Faculty of Medicine, The University of Hong Kong. The animals were randomized from different litters into experimental groups, and the animals were acclimatized at the BSL3 facility for 4-6 days prior to the experiments. The study protocol have been reviewed and approved by the Committee on the Use of Live Animals in Teaching and Research, The University of Hong Kong (CULATR # 5323-20). Experiments were performed in compliance with all relevant ethical regulations. For challenge studies, hamsters were anesthetized by ketamine(150mg/kg) and xylazine (10mg/kg) via intra-peritoneal injection and were intra-nasally inoculated with 8×10^4 TCID$_{50}$ of SARS-CoV-2 in 80 µL DMEM. On days 2, 5, 7, three hamsters were euthanized by intra-peritoneal injection of pentobarbital at 200mg/kg. No blinding was done and a sample size of three animals was selected to assess the level of variation between animals. Lungs (left) and one kidney were collected for viral load determination and were homogenized in 1mL PBS. Brain, nasal turbinate, lungs (right, liver, heart, spleen, duodenum, and kidney were fixed in 4% paraformaldehyde for histopathological examination. To collect fecal samples, hamsters were transferred to a new cage one day in advance and fresh fecal samples (10 pieces) were collected for quantitative real-time RT-PCR and TCID50 assay. To evaluate SARS-CoV-2 transmissibility by direct contact, donor hamsters were anesthetized and inoculated with 8×10^4 TCID$_{50}$ of SARS-CoV-2. On 1 dpi or on 6 dpi, one inoculated donor was transferred to co-house with one naïve hamster in a clean cage and co-housing of the animals continued for at least 13 days. Experiments were repeated with three pairs of donors: direct contact at 1:1 ratio[31,32]. Body weight and clinical signs of the animals were monitored daily. To evaluate SARS-CoV-2 transmissibility via aerosols, one naïve hamster was exposed to one inoculated donor hamster in two adjacent stainless steel wired cages on 1 dpi for 8 hours (Extended Data Fig. 3). DietGel®76A (ClearH$_2$O®) was provided to the hamsters during the 8-hour exposure. Exposure was done by holding the animals inside individually ventilated cages (IsoCage N, Techniplast) with 70 air changes per hour. Experiments were repeated with three pairs of donors: aerosol contact at 1:1 ratio. After exposure, the animals were single-housed in separate cages and were continued monitored for 14 days. To evaluate transmission potential of SARS-CoV-2 virus via fomites, three naïve fomite contact hamsters were each introduced to a soiled donor cage on 2 dpi. The fomite contact hamsters were single-housed for 48 hours inside the soiled cages and then were each transferred to a new cage on 4 dpi of the donor. All animals were continued monitored for 14 days. For nasal wash collection, hamsters were anesthetized by ketamine (100mg/kg) and xylazine (10mg/kg) via intra-peritoneal injection and 160 µL of PBS containing 0.3% BSA was used to collect nasal washes from both nostrils of each animal. Collected nasal washes were diluted 1:1 by volume and aliquoted for TCID$_{50}$ assay in Vero E6 cells and for quantitative real-time RT-PCR. The contact hamster were handled first followed by surface decontamination using 1% virkon and handling of the donor hamster.

Environmental sampling

To monitor the level of fomite contamination of SARS-CoV-2 virus in soiled cages, surface samples (5 cm x 5 cm, except that the whole water bottle nozzle was swabbed) were collected using flocked polyester swabs (Puritan). Swabs were stored in 0.5 mL of viral transport medium (VTM, containing 0.45% bovine serum albumin, vancomycin, amikacin and nystatin) at -80 °C. In addition, ten pieces of corn cob bedding were collected from the soiled cage and were soaked in 1 ml VTM for 30 minutes before titration of infectious virus and viral RNA extraction. Infectious viral loads were determined in Vero E6 cells, and viral RNA copy numbers were determined by quantitative real-time RT-PCR.

Viral load determination by quantitative real-time RT-PCR

RNA was extracted from 140 µL samples using QIAamp viral RNA mini kit (Qiagen) and eluted with 60 µL of water. Two µL RNA was used for real-time qRT-PCR to detect and quantified N gene of SARS-CoV-2 using TaqMan™ Fast Virus 1-Step Master Mix as described[33].

Plaque reduction neutralization (PRNT) assay

The experiments were carried out in duplicate using Vero E6 cells seeded in 24-well culture plates. Serum samples were heat-inactivated at 56 °C for 30 min and were serially diluted and incubated with 30–40 plaque-forming units of SARS-CoV-2 for 1 h at 37 °C. The virus–serum mixtures were added to the cells and incubated 1 h at 37 °C in 5% CO$_2$ incubator. The plates were overlaid with 1% agarose in cell culture medium and incubated for 3 days. Thereafter the plates were fixed and stained with 1% crystal violet. Antibody titres were defined as the highest serum dilution that resulted in > 90% (PRNT$_{90}$) reduction in the number of plaques.

Histopathology and immunohistochemistry

Tissue (hearts, livers, spleens, duodenums, brains, right lungs and kidneys) were fixed in 4% paraformaldehyde and were processed for paraffin embedding. The 4-µm sections were stained with hematoxylin and eosin for histopathological examinations. For immunohistochemistry, SARS-CoV-2 N protein was detected using monoclonal antibody (4D11)[34], CD3 was detected using polyclonal rabbit anti-human CD3 antibodies (DAKO), and the neuron-specific beta-III tubulin was detected using monoclonal antibody clone TuJ1 (R&D Systems). Images were captured using a Leica DFC 5400 digital camera and were processed using Leica Application Suite v4.13.

Statistics and reproducibility

Kruskal-Wallis test and Dunn's multiple comparisons test were used to compare viral loads in the lungs and kidney on 2, 5, 7 dpi. Area under the curve was calculated from the nasal washes of the donor and contact hamsters followed by Mann-Whiteny test. Data were analyzed in Microsoft Excel for Mac, version 16.35 and GraphPad Prism version 8.4.1. For the detection viral replication in hamsters, 9 hamsters were inoculated and tissues were collected from animals on 2 (N=3), 5 (N=3), 7 (N=3) dpi; the results from the three animals were similar (Fig. 1a and 1b). Inoculation of the donor hamsters was independently performed twice and the inoculated hamsters showed comparable weight loss and shed comparable amount of virus in the nasal washes (Fig. 2a, 2b, 3a, 3b). Transmission by direct contact, via aerosols or fomites were performed with three pairs of donor: contacts at 1:1 ratio.

Reporting summary

Further information on research design is available in the Nature Research Reporting Summary linked to this paper.

Data availability

The sequence of SARS-CoV-2 virus BetaCoV/Hong Kong/VM20001061/2020 can be accessed at www.gisaid.org (EPI_ISL_412028).

Article

All experimental data shown in Figures 1, 2, 3, Extended Data Figures 2, and Extended Data Table 1 are available from the authors upon request.

31. Belser, J. A., Maines, T. R., Katz, J. M. & Tumpey, T. M. Considerations regarding appropriate sample size for conducting ferret transmission experiments. *Future Microbiol* **8**, 961-965, https://doi.org/10.2217/fmb.13.64 (2013).

32. Nishiura, H., Yen, H. L. & Cowling, B. J. Sample size considerations for one-to-one animal transmission studies of the influenza A viruses. *PLoS One* **8**, e55358, https://doi.org/10.1371/journal.pone.0055358 (2013).

33. Chu, D. K. W. *et al*. Molecular Diagnosis of a Novel Coronavirus (2019-nCoV) Causing an Outbreak of Pneumonia. *Clin Chem*, https://doi.org/10.1093/clinchem/hvaa029 (2020).

34. Nicholls, J. M. *et al*. Time course and cellular localization of SARS-CoV nucleoprotein and RNA in lungs from fatal cases of SARS. *PLoS Med* **3**, e27, https://doi.org/10.1371/journal.pmed.0030027 (2006).

35. Lan, J. *et al*. Structure of the SARS-CoV-2 spike receptor-binding domain bound to the ACE2 receptor. *Nature*, https://doi.org/10.1038/s41586-020-2180-5 (2020).

36. Li, W. *et al*. Receptor and viral determinants of SARS-coronavirus adaptation to human ACE2. *EMBO J* **24**, 1634-1643, https://doi.org/10.1038/sj.emboj.7600640 (2005).

Author contributions SFS, LMY, AWC, HLY designed and performed the experiments; KTC, AYLW, PK, RAP performed the experiments, KF and JMN performed immunohistochemistry and histopathological examination; LLMP, JMN, MP, and HLY analysed the data and wrote the manuscript.

Competing interests The authors declare no competing interests.

Additional information
Supplementary information is available for this paper at https://doi.org/10.1038/s41586-020-2342-5.
Correspondence and requests for materials should be addressed to H.-L.Y.
Peer review information *Nature* thanks Emmie de Wit, Stanley Perlman and the other, anonymous, reviewer(s) for their contribution to the peer review of this work. Peer reviewer reports are available.
**Reprints and permissions information** is available at http://www.nature.com/reprints.

```
                    10         20         30         40         50         60         70
             ....|....|....|....|....|....|....|....|....|....|....|....|....|....|
Human ACE2   MSSSSWLLLSLVAVTAAQSTIEEQAKTFLDKFNHEAEDLFYQSSLASWNYNTNITEENVQMNNAGDKWS
Macaca ACE2  MSGSSWLLLSLVAVTAAQSTIEEQAKTFLDKFNHEAEDLFYQSSLASWNYNTNITEENVQMNNAGEKWS
Hamster ACE2 MSSSSWLLLSLVAVTTAQSIIEEQAKTFLDKFNQEAEDLSYQSALASWNYNTNITEENAQKMNEAAAKWS
Mouse ACE2   MSSSSWLLLSLVAVTTAQSLTEENAKTFLNNFNQEAEDLSYQSSLASWNYNTNITEENAQKMSEAAAKWS
                     *   **  **    **   **    **   *

                    80         90        100        110        120        130        140
             ....|....|....|....|....|....|....|....|....|....|....|....|....|....|
Human ACE2   AFLKEQSTLAQMYPLQEIQNLTVKLQLQALQQNGSSVLSEDKSKRLNTILNTMSTIYSTGKVCNPDNPQE
Macaca ACE2  AFLKEQSTLAQMYPLQEIQNLTVKLQLQALQQNGSSVLSEDKSKRLNTILNTMSTIYSTGKVCNPNNPQE
Hamster ACE2 AFYEEQSKLAKNYSLQEVQNLTIKRQLQALQQSGSSALSADKNKQLNTILNTMSTIYSTGKVCNPKNPQE
Mouse ACE2   AFYEEQSKTAQSFSLQEIQTPIIKRQLQALQQSGSSALSADKNKQLNTILNTMSTIYSTGKVCNPKNPQE
                       **

                   150        160        170        180        190        200        210
             ....|....|....|....|....|....|....|....|....|....|....|....|....|....|
Human ACE2   CLLLEPGLNEIMANSLDYNERLWAWESWRSEVGKQLRPLYEEYVVLKNEMARANHYEDYGDYWRGDYEVN
Macaca ACE2  CLLLDPGLNEIMEKSLDYNERLWAWEGWRSEVGKQLRPLYEEYVVLKNEMAGANHYKDYGDYWRGDYEVN
Hamster ACE2 CLLLEPGLDDIMATSTDYNERLWAWEGWRAEVGKQLRPLYEEYVVLKNEMARANNYEDYGDYWRGDYEAE
Mouse ACE2   CLLLEPGLDEIMATSTDYNSRLWAWEGWRAEVGKQLRPLYEEYVVLKNEMARANNYNDYGDYWRGDYEAE

                   220        230        240        250        260        270        280
             ....|....|....|....|....|....|....|....|....|....|....|....|....|....|
Human ACE2   GVDGYDYSRGQLIEDVEHTFEEIKPLYEHLHAYVRAKLMNAYPSYISPIGCLPAHLLGDMWGRFWTNLYS
Macaca ACE2  GVDGYDNNRDQLIEDVERTFEEIKPLYEHLHAYVRAKLMNAYPSYISPTGCLPAHLLGDMWGRFWTNLYS
Hamster ACE2 GADGYNYNGNQLIEDVERTFKEIKPLYEQLHAYVRTKLMNTYPSYISPTGCLPAHLLGDMWGRFWTNLYP
Mouse ACE2   GADGYNYNRNQLIEDVERTFAEIKPLYEHLHAYVRRKLMDTYPSYISPTGCLPAHLLGDMWGRFWTNLYP

                   290        300        310        320        330        340        350
             ....|....|....|....|....|....|....|....|....|....|....|....|....|....|
Human ACE2   LTVPFGQKPNIDVTDAMVDQAWDAQRIFKEAEKFFVSVGLPNMTQGFWENSMLTDPGNVQKAVCHPTAWD
Macaca ACE2  LTVPFGQKPNIDVTDAMVNQAWNAQRIFKEAEKFFVSVGLPNMTQGFWENSMLTDPGNVQKVVCHPTAWD
Hamster ACE2 LTVPFGQKPNIDVTDAMVNQGWNAERIFKEAEKFFVSVGLPYMTQGFWENSMLTDPGDDRKVVCHPTAWD
Mouse ACE2   LTVPFAQKPNIDVTDAMMNQGWDAERIFQEAEKFFVSVGLPHMTQGFWANSMLTEPADGRKVVCHPTAWD
                                                       *

                   360        370        380        390        400        410        420
             ....|....|....|....|....|....|....|....|....|....|....|....|....|....|
Human ACE2   LGKGDFRILMCTKVTMDDFLTAHHEMGHIQYDMAYAAQPFLLRNGANEGFHEAVGEIMSLSAATPKHLKS
Macaca ACE2  LGKGDFRIIMCTKVTMDDFLTAHHEMGHIQYDMAYAAQPFLLRNGANEGFHEAVGEIMSLSAATPKHLKS
Hamster ACE2 LGKGDFRIKMCTKVTMDNFLTAHHEMGHIQYDMAYATQPFLLRNGANEGFHEAVGEIMSLSAATPEHLKS
Mouse ACE2   LGHGDFRIKMCTKVTMDNFLTAHHEMGHIQYDMAYARQPFLLRNGANEGFHEAVGEIMSLSAATPKHLKS
               ***  *                                      *
```

Extended Data Fig. 1 | Sequence alignment of ACE2 proteins (1-420) from human, macaca, hamster, and mouse. Amino acid residues of human ACE2 that are experientially shown to interact with the receptor binding domain (RBD) of SARS-CoV-2[35] are denoted by *. Amino acid residues that are important for the interaction between human ACE2 and RBD of SARS-CoV are highlighted in red boxes[36].
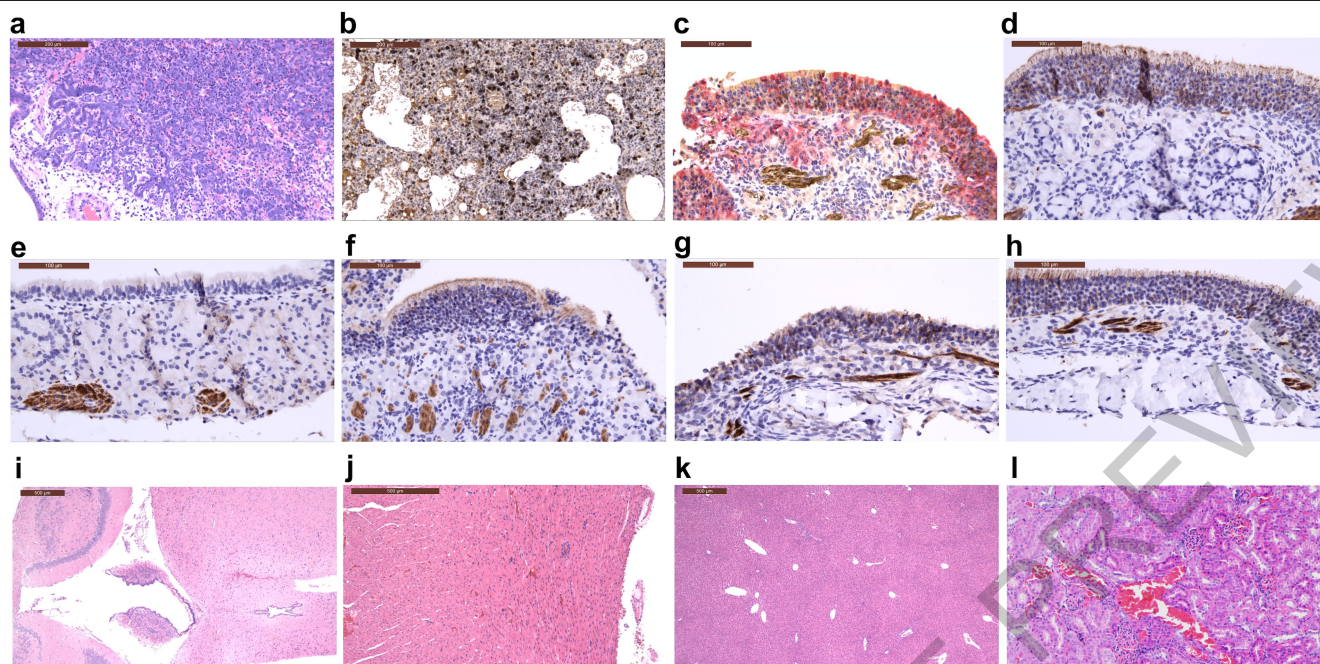
Extended Data Fig. 2 | Haemotoxylin and eosin (H&E) staining and immunohistochemistry on SARS-CoV-2 challenged hamster tissues. **a**, Hyperplasia of the pneumocytes detected on 7 dpi. **b**, Detection of CD3 positive cells (using rabbit anti-human CD3 polyclonal antibody) in the lungs on 5 dpi. **c**, Detection of SARS-CoV-2 N protein (red staining, using monoclonal antibody 4D11) and olfactory neurons (brown staining, using monoclonal antibody TuJ1) from the nasal turbinate on 5 dpi. **d**, Detection of olfactory neurons (using monoclonal antibody TuJ1) from the nasal turbinate of a mock infected hamster (N=1). **e**, Nasal epithelial cells from the nasal turbinate of a mock infected hamster (N=1) showed negative staining for TuJ1. **f**, Detection of olfactory neurons from nasal turbinate on 2 dpi. **g**, Detection of olfactory neurons from nasal turbinate on 7 dpi. **h**, Detection of olfactory neurons from nasal turbinate on 14 dpi. **i**, H&E staining of the brain tissue on 5 dpi. **j**, H&E staining of the heart on 5 dpi. **k**, H&E staining of the liver on 5 dpi. **l**, H&E staining of the kidney on 5 dpi. Hamsters were intra-nasally inoculated with PBS (mock infection, N=1) or with 8×10^4 TCID$_{50}$ of SARS-CoV-2 (N=9) and the tissues were collected on 2 (N=3), 5 (N=3), 7 (N=3) dpi. H&E and immunohistochemistry with tissues from three animals showed similar results and the representative results were shown.
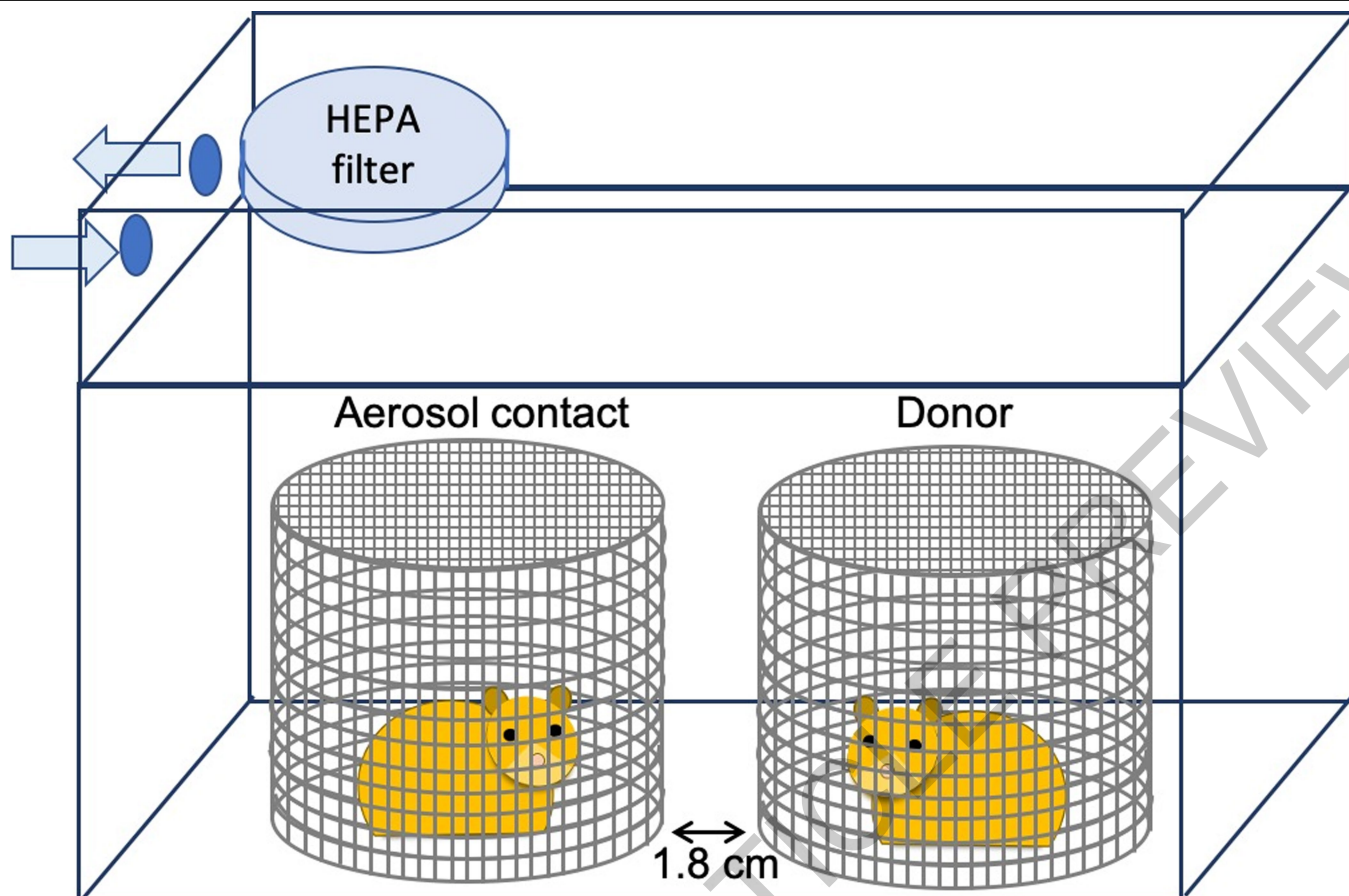
Extended Data Fig. 3 | Experimental layout for the aerosol transmission experiment in hamsters. To evaluate SARS-CoV-2 transmissibility via aerosols, one naïve hamster was exposed to one inoculated donor hamster in two adjacent stainless steel wired cages on 1 dpi for 8 hours. DietGel®76A (ClearH₂O®) was provided to the hamsters during the 8-hour exposure. Exposure was done by holding the animals inside individually ventilated cages (IsoCage N, Techniplast) with 70 air changes per hour. Experiments were repeated with three pairs of donors: aerosol contact at 1:1 ratio. After exposure, the animals were single-housed in separate cages and were continued monitored for 14 days.

Article

Extended Data Table 1 | Detection of SARS-CoV-2 in the soiled cages

Days post-inoculation	Animal cage info	Sampled area	Material	$\log_{10}$ TCID$_{50}$/ mL	$\log_{10}$ RNA copies/ mL
Day 2	donor cage A			**1.79**	**6.70**
	donor cage B	bedding	corn cobs	<	5.18
	donor cage C			<	5.79
Day 4	fomite contact cage A	cage side (in direct contact with the animals)	plastic	<	6.89
	fomite contact cage B			<	5.21
	fomite contact cage C			**1.79**	**6.33**
	fomite contact cage A	cage lid	plastic	<	3.76
	fomite contact cage B			<	4.33
	fomite contact cage C			<	4.10
	fomite contact cage A	pre-filter	paper-based	<	5.26
	fomite contact cage B			<	5.27
	fomite contact cage C			<	5.31
	fomite contact cage A	water bottle nozzle	stainless steel	<	3.64
	fomite contact cage B			<	4.20
	fomite contact cage C			**2.21**	**6.06**
	fomite contact cage A	bedding	corn cobs	<	4.84
	fomite contact cage B			<	5.27
	fomite contact cage C			<	6.06
Day 6	fomite contact cage A	cage side (in direct contact with the animals)	plastic	<	5.70
	fomite contact cage B			<	5.61
	fomite contact cage C			<	6.51
	fomite contact cage A	cage lid	plastic	<	4.75
	fomite contact cage B			<	3.46
	fomite contact cage C			<	4.24
	fomite contact cage A	pre-filter	paper-based	<	5.48
	fomite contact cage B			<	5.23
	fomite contact cage C			<	5.36
	fomite contact cage A	bedding	corn cobs	<	5.12
	fomite contact cage B			<	6.24
	fomite contact cage C			<	5.58

To evaluate transmission potential of SARS-CoV-2 virus via fomites, three naïve fomite contact hamsters were each introduced to a soiled donor cage on 2 dpi. The fomite contact hamsters were single-housed for 48 hours inside the soiled cages and then were each transferred to a new cage on 4 dpi of the donors. The soiled cages were left empty at room temperature and were sampled again on 6 dpi of the donor. Surface samples and corn cob bedding were collected from the soiled cages on different time points to monitor infectious viral load and viral RNA copy numbers in the samples.

nature research

Corresponding author(s): Hui-Ling Yen

Last updated by author(s): May 1, 2020

Reporting Summary

Nature Research wishes to improve the reproducibility of the work that we publish. This form provides structure for consistency and transparency in reporting. For further information on Nature Research policies, see Authors & Referees and the Editorial Policy Checklist.

Statistics

For all statistical analyses, confirm that the following items are present in the figure legend, table legend, main text, or Methods section.

n/a	Confirmed	
☐	☒	The exact sample size (*n*) for each experimental group/condition, given as a discrete number and unit of measurement
☐	☒	A statement on whether measurements were taken from distinct samples or whether the same sample was measured repeatedly
☐	☒	The statistical test(s) used AND whether they are one- or two-sided *Only common tests should be described solely by name; describe more complex techniques in the Methods section.*
☒	☐	A description of all covariates tested
☒	☐	A description of any assumptions or corrections, such as tests of normality and adjustment for multiple comparisons
☐	☒	A full description of the statistical parameters including central tendency (e.g. means) or other basic estimates (e.g. regression coefficient) AND variation (e.g. standard deviation) or associated estimates of uncertainty (e.g. confidence intervals)
☐	☒	For null hypothesis testing, the test statistic (e.g. *F*, *t*, *r*) with confidence intervals, effect sizes, degrees of freedom and *P* value noted *Give P values as exact values whenever suitable.*
☒	☐	For Bayesian analysis, information on the choice of priors and Markov chain Monte Carlo settings
☒	☐	For hierarchical and complex designs, identification of the appropriate level for tests and full reporting of outcomes
☒	☐	Estimates of effect sizes (e.g. Cohen's *d*, Pearson's *r*), indicating how they were calculated

Our web collection on statistics for biologists contains articles on many of the points above.

Software and code

Policy information about availability of computer code

Data collection	Experimental data were recorded in Microsoft Excel for Mac, version 16.35. Images were captured using a Leica DFC 5400 digital camera and were processed using Leica Application Suite v4.13
Data analysis	Data were analyzed in Microsoft Excel for Mac, version 16.35 and GraphPad Prism version 8.4.1.

For manuscripts utilizing custom algorithms or software that are central to the research but not yet described in published literature, software must be made available to editors/reviewers. We strongly encourage code deposition in a community repository (e.g. GitHub). See the Nature Research guidelines for submitting code & software for further information.

Data

Policy information about availability of data

All manuscripts must include a data availability statement. This statement should provide the following information, where applicable:

- Accession codes, unique identifiers, or web links for publicly available datasets
- A list of figures that have associated raw data
- A description of any restrictions on data availability

The accession number for the SARS-CoV-2 virus used for the study was provided.
There are two figures that have associated raw data. All data will be provided upon request.

Field-specific reporting

Please select the one below that is the best fit for your research. If you are not sure, read the appropriate sections before making your selection.

☒ Life sciences ☐ Behavioural & social sciences ☐ Ecological, evolutionary & environmental sciences

For a reference copy of the document with all sections, see nature.com/documents/nr-reporting-summary-flat.pdf

Life sciences study design

All studies must disclose on these points even when the disclosure is negative.

Sample size	This is an observational study investigates the suitability of using golden Syrian hamsters as an animal model for SARS-CoV-2. There is no comparison to be made with another virus, and a sample size of 3 was selected to evaluate the level of variation between individuals. Transmission studies are generally performed in 3-4 pairs of donor: contact at 1:1 ratio (Nishura et al., PLOS ONE 2013 and Belser et al., Future Microbiol 2013).
Data exclusions	No data was excluded in the analyses.
Replication	The challenge experiment was repeatedly performed three times. Direct contact transmission experiments were independently performed twice and naive animals were co-housed with inoculated donors on day 1 and day 6, respectively. Each experiment was performed with three pairs of donor: contact at 1:1 ratio. Aerosol transmission and fomite transmission experiments were each performed once with three pairs of donor: contact at 1:1 ratio.
Randomization	Randomization was performed while assigning the animals from different litters into experimental groups.
Blinding	Blinding was not possible for the experimental design due to the need to identify each animal (inoculated or contact) accurately.

Reporting for specific materials, systems and methods

We require information from authors about some types of materials, experimental systems and methods used in many studies. Here, indicate whether each material, system or method listed is relevant to your study. If you are not sure if a list item applies to your research, read the appropriate section before selecting a response.

Materials & experimental systems

n/a	Involved in the study
☐	☒ Antibodies
☐	☒ Eukaryotic cell lines
☒	☐ Palaeontology
☐	☒ Animals and other organisms
☒	☐ Human research participants
☒	☐ Clinical data

Methods

n/a	Involved in the study
☒	☐ ChIP-seq
☒	☐ Flow cytometry
☒	☐ MRI-based neuroimaging

Antibodies

Antibodies used	SARS-CoV-2 N protein was detected using monoclonal antibody (4D11). CD3 was detected using polyclonal rabbit anti-human CD3 antibody purchased from DAKO. Neuron-specific beta-III tubulin was detected using monoclonal clone TuJ1 (R&D Systems).
Validation	4D11 monoclonal antibody was reported in Nicholls et al. PLoS Med. 2006 Feb;3(2):e27. PubMed PMID: 16379499 Other antibodies are available commercially.

Eukaryotic cell lines

Policy information about cell lines

Cell line source(s)	Vero E6 (ATCC CRL-1586)
Authentication	The cell line was purchased from ATCC (ATCC CRL-1586). The cell line has not been authenticated since it was purchased from ATCC.
Mycoplasma contamination	The cell line was tested negative for mycoplasma.
Commonly misidentified lines (See ICLAC register)	No commonly misidentified lines were used.

Animals and other organisms

Policy information about studies involving animals; ARRIVE guidelines recommended for reporting animal research

Laboratory animals	Male golden Syrian hamsters, at 4-5 weeks old
Wild animals	This study does not involve wild animals.
Field-collected samples	This study does not involve field-collected samples.
Ethics oversight	Animal ethics was approved by the the Committee on the Use of Live Animals in Teaching and Research, The University of Hong Kong (CULATR # 5323-20).

Note that full information on the approval of the study protocol must also be provided in the manuscript.